

Article

N,O Chelating Ligands Construct Five-Coordinated Zn(II) Exclusive {Zn₆} Clusters: Decomposition, Stepwise Assembly and Photoluminescence Study

Qian-Jun Deng *, Min Chen, Dong-Chu Chen * and Chang-Ai Chen

School of Material Science and Energy Engineering, Foshan University, Foshan 528000, Guangdong, China

* Correspondence: dqj39@fosu.edu.cn (Q.J.D.); Chendc@fosu.edu.cn (D.C.C.)

Received: 27 July 2019; Accepted: 11 August 2019; Published: 12 August 2019



Abstract: *N*-methylbenzimidazole-2-methanol (*Hmbm*) and Zn(NO₃)₂·6H₂O were reacted in acetonitrile solvothermal at 80 °C for 48 h to obtain a six-nuclear Zn(II) cluster ([Zn^{II}₆(*Hmbm*)₂(*mbm*)₈(NO₃)₄)]·12H₂O·2CH₃CN (**Zn6**). Structural analysis indicated that Zn(II) in the above **Zn6** clusters showed pentacoordinates. The metal centers Zn1 and Zn2 are both in the N₂O₃ coordination environment, and both show a triangular bipyramid configuration. Zn3 is in a NO₄ coordination environment, which is also shown as a triangular bipyramid configuration. The ion source voltage of high-resolution electrospray ionization mass spectrometry (HRESI-MS) was further adjusted to bombard the **Zn6** cluster, and seven major key intermediates were identified. Furthermore, we proposed that the gradual fragmentation mechanism is **Zn6** → [Zn^{II}₆(*mbm*)₈(NO₃)₃]⁺ → [Zn^{II}₅(*mbm*)₇(NO₃)₂]⁺ → [Zn^{II}₄(*mbm*)₆(NO₃)₁]⁺ → [Zn^{II}₃(*mbm*)₄(NO₃)₁]⁺ → [Zn^{II}₂(*mbm*)₃]⁺ → [Zn^{II}₂(*mbm*)₂(OH)(H₂O)₂(DMSO)]⁺ → [Zn^{II}(*mbm*)]⁺. In order to understand the gradual formation of **Zn6** clusters, herein, we track the changes of species in the solution in different time periods by HRESI-MS. The nine key intermediates were identified and further combined with its gradual fragmentation mechanism. We proposed the gradual assembly mechanism of [Zn^{II}(*mbm*)]⁺ → [Zn^{II}(*mbm*)(*Hmbm*)]⁺ → [Zn^{II}₂(*mbm*)₂(NO₃)₁]⁺ → [Zn^{II}₂(*mbm*)₃]⁺ → [Zn^{II}₃(*mbm*)₄(NO₃)₁]⁺ → [Zn^{II}₄(*mbm*)₅(NO₃)₂]⁺ → [Zn^{II}₄(*mbm*)₆(NO₃)₁]⁺ → [Zn^{II}₅(*mbm*)₇(NO₃)₂]⁺ → [Zn^{II}₆(*mbm*)₈(NO₃)₃]⁺ → **Zn6**. To the best of our knowledge, this is the first time that a decomposition and assembly binding strategy has been used to resolve the stepwise formation of Zn(II) clusters. Photoluminescence measurements indicate that the cluster **Zn6** exhibits a strong emission peak at 300 nm and an emission shoulder at 600 nm.

Keywords: N,O chelating ligands; five-coordinated Zn(II) Exclusive {Zn₆} clusters; decomposition; stepwise assembly; photoluminescence

1. Introduction

An important goal in chemistry is to define the precise mechanisms of chemical reactions and to apply this knowledge to the preparation of molecules with novel structures and functions [1–14]. The cluster of coordination molecules is typically formed and crystallized in a hydrothermal/solvent heat sealing system with a certain temperature and pressure [4,5]. To date, a major challenge in coordination chemistry is to accurately detect and identify major component changes in complex coordination molecule cluster formation processes, track their behavior in solution, and finally analyze their self-assembly mechanisms [8–10]. The study of the assembly mechanism of coordination molecular clusters is essential for revealing their chemical reactivity and extending their inherent properties such as potential applications [4,6,7]. Due to limited research methods, technical means, and research tools, the assembly mechanism of coordination molecular clusters in hydrothermal/solvothermal

“closed” systems has been extremely difficult to explore [4,5,9–13]. Although the formation process and assembly mechanism are very complicated, at present, some significant progress has been made in the assembly mechanism of heteropolyacids, the coordination supramolecular systems and molecular cages, and the lanthanide coordination cluster [9–21].

Faced with the above challenges, it is important to choose the right strategy and method [10]. Inverse synthesis analysis has received extensive attention as an important strategy for organic synthesis. We believe that if a certain amount of energy is applied to the coordination molecule cluster to cause stepwise fragmentation, since the order of the fragmentation of clusters is related to the strength of the coordination bond, we can judge and speculate the self-assembly process (similar to inverse synthesis analysis) by stepwise cleavage of the cluster. Further incorporation of the critical intermediates tracked and identified by the cluster formation process is highly helpful in the inference of its assembly mechanism.

Herein, we used the N,O chelating ligand *N*-methylbenzimidazole-2-methanol (*Hmbm*) to react with $\text{Zn}(\text{NO}_3)_2 \cdot 6\text{H}_2\text{O}$ under solvothermal conditions to achieve the synthesis of the hexa-nuclear Zn(II) cluster ($[\text{Zn}^{\text{II}}_6(\text{Hmbm})_2(\text{mbm})_8(\text{NO}_3)_4] \cdot 12\text{H}_2\text{O} \cdot 2\text{CH}_3\text{CN}$ (**Zn6**)). The six Zn(II) in the cluster **Zn6** adopts a five-coordinated coordination mode. In the high-resolution electrospray mass spectrometry (HRESI-MS) test of **Zn6**, we found that it could be easily broken. Therefore, we adjusted the voltage of different ion sources to cause the gradual decomposition of **Zn6**, and by further combining the key intermediates and strength changes that occur during the assembly process, we proposed a **Zn6** assembly mechanism. To the best of our knowledge, this is the first study of the self-assembly mechanism of Zn(II) clusters by means of decomposition and assembly. Finally, a photoluminescence test of **Zn6** showed that it mainly showed the π – π^* energy level transition of the ligand and showed blue-green light emission.

2. Results and Discussion

2.1. Crystal Structure

X-ray single crystal diffraction results indicate that the cluster **Zn6** crystallizes in the space group $P2_1/c$ (Supplementary Materials Tables S1 and S2). The cluster **Zn6** consists of six Zn^{2+} ions, ten ligands, and four nitrates, respectively (Figure 1a). There are twelve water molecules and two acetonitrile molecules free on the periphery of the cluster **Zn6**. The six Zn(II) in the cluster **Zn6** are each bridged by eight oxygen from the ligand (six μ_2 and two μ_3) (Figure 1b). There are three different coordination environments of Zn(II) in the **Zn6** structure, but the above three Zn(II) are all five-coordination. They are (Figure 1c–h): (1) Zn1 forms a pentacoordinate with three O atoms and two N atoms from three different ligands; (2) Zn2 forms a pentacoordinate with three O atoms and two N atoms from three different ligands, respectively; and (3) although Zn3 also forms pentacoordinates with three O atoms and two N atoms from three different ligands, the coordination configuration is different. For Zn1, the Zn–O distance ranges from 2.00 Å to 2.33 Å, and the Zn–N distance is from 1.99 Å to 2.01 Å, and the above distances are within the normal range (Table S2). By using *SHAPE*, the calculation results showed that Zn1 with a N_3O_2 coordination environment exhibits a trigonal bipyramid configuration (Table S3). Further analysis of the coordination environment of Zn2 showed that the Zn–O distance ranged from 1.98 Å to 2.26 Å, and the distance of Zn–N was 2.00 Å to 2.08 Å. By using *SHAPE*, the calculation results showed that Zn2, which also has a N_3O_2 coordination environment, also exhibits a trigonal bipyramid configuration. Finally, Zn3 is in a NO_4 coordination environment with a Zn–O distance ranging from 1.98 Å to 2.25 Å and a Zn–N distance of 2.04 Å. By using *SHAPE*, the calculations showed that the five-coordinated Zn3 showed a trigonal bipyramid configuration. In order to further understand the crystal growth process of **Zn6**, we analyzed the weak effect of **Zn6** (Table S4, Figure S1). There are two main hydrogen bonds between **Zn6** and free NO_3^- during the stacking of **Zn6** clusters: (1) $\text{O}_5\text{--H}_5 \cdots \text{O}_8$ (pink dotted line), the distance between $\text{H}_5 \cdots \text{O}_8$ is 1.81 Å, $\angle \text{O}_5\text{H}_5\text{O}_8 = 168^\circ$; and (2) $\text{C}_{32}\text{--H}_{32} \cdots \text{O}_9$ (gray dotted line), $\text{H}_{32} \cdots \text{O}_9$ has a distance of 2.60 Å, $\angle \text{C}_{32}\text{H}_{32}\text{O}_9 = 161^\circ$. In addition

to hydrogen bonding, there are two weak effects of $N-O \cdots \pi$: (1) $N_{12}-O_9 \cdots \text{PhC}_3\text{N}_2$ (golden dotted line), where the distance from O_9 to the imidazole ring (PhC_3N_2) is 3.44 Å; and (2) $N_{12}-O_{10} \cdots \text{PhC}_3\text{N}_2$ (blue dotted line), where the distance from O_{10} to the imidazole ring is 3.34 Å. There is an $O-H \cdots \pi$ interaction between the cluster **Zn6** and the free water molecules (pink dotted line), where the distance from H to the plane of the benzene ring is 2.60 Å. In addition, there is a $\pi \cdots \pi$ interaction between the **Zn6** molecules with a distance of 3.47 Å (black dashed line). All of the above weak effects are very important for the growth process of **Zn6** crystals, which form a three-dimensional network. Six **Zn6** clusters are connected around one **Zn6** cluster, and the three-dimensional stacking method is arranged according to “AAA” (Figure S2).

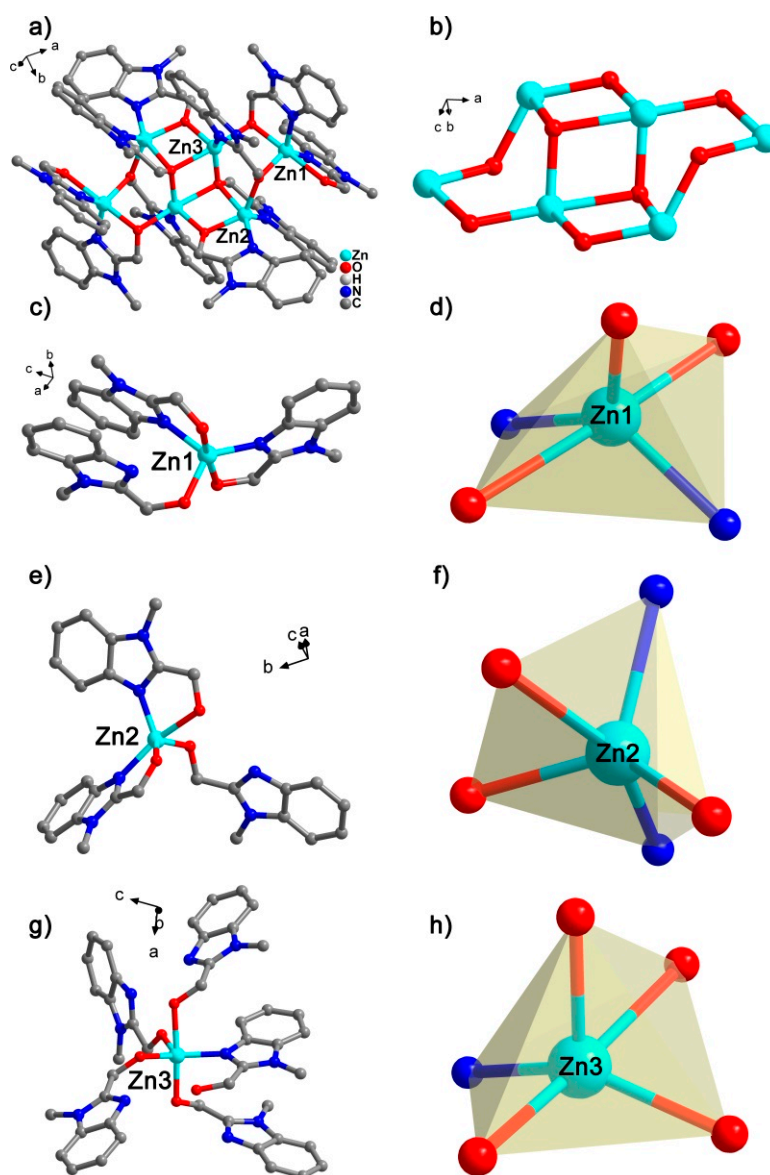


Figure 1. (a) Crystal structure of complex **Zn6**; (b) cluster nucleus Zn_6O_8 structure, where all H, C, and N atoms are omitted for clarity; coordination environment (c,e,g) and coordination configuration (d,f,h) of Zn1, Zn2, and Zn3.

The experimental values of the powder diffraction pattern of the cluster **Zn6** at room temperature are in good agreement with the fitted values, which proved that a large amount of **Zn6** synthesized in the experiment was a pure phase (Figure S3a). The thermogravimetric analysis (TGA) curve of **Zn6** was further tested, and the results showed that it had two significant weight losses during the heating

process (Figure S3b). The first weight loss was in the range of 35–86 °C, which can be attributed to twelve free water molecules. In theory, the weight loss was 8.5% (actual weight loss 8.3%). The second weight loss was in the range of 202–264 °C, which can be attributed to two free acetonitrile molecules, theoretically losing 3.2% (actual weight loss of 3.4%). This is consistent with the free solvent present in the **Zn6** structure.

2.2. High Resolution Electrospray Ionization Mass Spectrometry

The research on the assembly mechanism of high nuclear clusters has always been a hot spot in coordination chemistry. The gradual fragmentation of high-nuclear clusters with a certain amount of energy will provide a very important basis for the study of its assembly mechanism, so it will be helpful to guess the intermediate fragments in the formation process. Therefore, we selected clean **Zn6** crystals dissolved in chromatographically pure dimethyl sulfoxide (DMSO) and diluted with acetonitrile for high-resolution electrospray mass spectrometry (HRESI-MS) to collect data in the m/z range of 200–2000 in both positive and negative modes (Figures S4–S7, Table S5). As shown in Figure 2, when the energy of the ion source was 0 eV, the main frame peak of **Zn6** was not observed, and the g fragment with the peak abundance of $m/z = 1866.10$ was captured, which could be classified as $[\text{Zn}^{\text{II}}_6(\text{mbm})_8(\text{NO}_3)_3]^+$ (fit 1866.10). The production of the above fragments was caused by the loss of two Hmbm ligands at the periphery of **Zn6**. In addition, the c fragment with the strongest peak abundance $m/z = 613.07$, the d segment with the second strongest peak $m/z = 902.06$, and the b segment with very low intensity $m/z = 585.06$ were observed. Finally, an e fragment of $m/z = 1290.13$ and an f fragment of $m/z = 1579.11$ were observed. The above fragments could be assigned to $[\text{Zn}^{\text{II}}_2(\text{mbm})_3]^+$ (fit 613.07), $[\text{Zn}^{\text{II}}_3(\text{mbm})_4(\text{NO}_3)]^+$ (fit 902.10), $[\text{Zn}^{\text{II}}_2(\text{mbm})_2(\text{OH})(\text{H}_2\text{O})_2(\text{DMSO})]^+$ (fit 583.06), $[\text{Zn}^{\text{II}}_4(\text{mbm})_6(\text{NO}_3)]^+$ (fit 1290.13), and $[\text{Zn}^{\text{II}}_5(\text{mbm})_7(\text{NO}_3)_2]^+$ (fit 1579.11). The above results indicate that the structure of **Zn6** is unstable and it is easily broken into other small-nuclear species fragments under certain energy conditions. In order to further clearly analyze the fracture mode of **Zn6**, we conducted a HRESI-MS test under different ion source energies (0–100 eV). It can be seen that as the energy increased, the intensity of the high-nuclear species fragments gradually decreased (such as c, d, e, f, and g), while the peak intensity of the low-nuclear species fragments gradually increased (such as $[\text{Zn}^{\text{II}}(\text{mbm})]^+$ (fit 225.00), a), so we believe that the fracture process mechanism of **Zn6** is $[\text{Zn}^{\text{II}}_6(\text{Hmbm})_2(\text{mbm})_8(\text{NO}_3)_4] (\text{Zn6}) \rightarrow [\text{Zn}^{\text{II}}_6(\text{mbm})_8(\text{NO}_3)_3]^+ \rightarrow [\text{Zn}^{\text{II}}_5(\text{mbm})_7(\text{NO}_3)_2]^+ \rightarrow [\text{Zn}^{\text{II}}_4(\text{mbm})_6(\text{NO}_3)]^+ \rightarrow [\text{Zn}^{\text{II}}_3(\text{mbm})_4(\text{NO}_3)]^+ \rightarrow [\text{Zn}^{\text{II}}_2(\text{mbm})_3]^+ \rightarrow [\text{Zn}^{\text{II}}_2(\text{mbm})_2(\text{OH})(\text{H}_2\text{O})_2(\text{DMSO})]^+ \rightarrow [\text{Zn}^{\text{II}}(\text{mbm})]^+$.

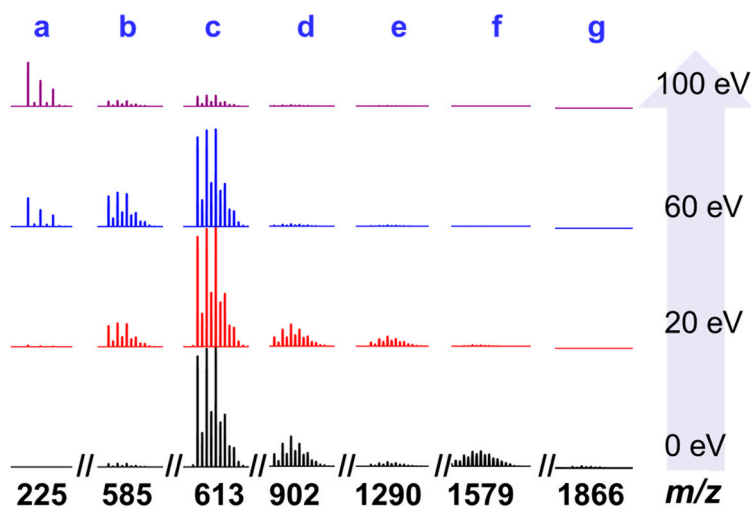
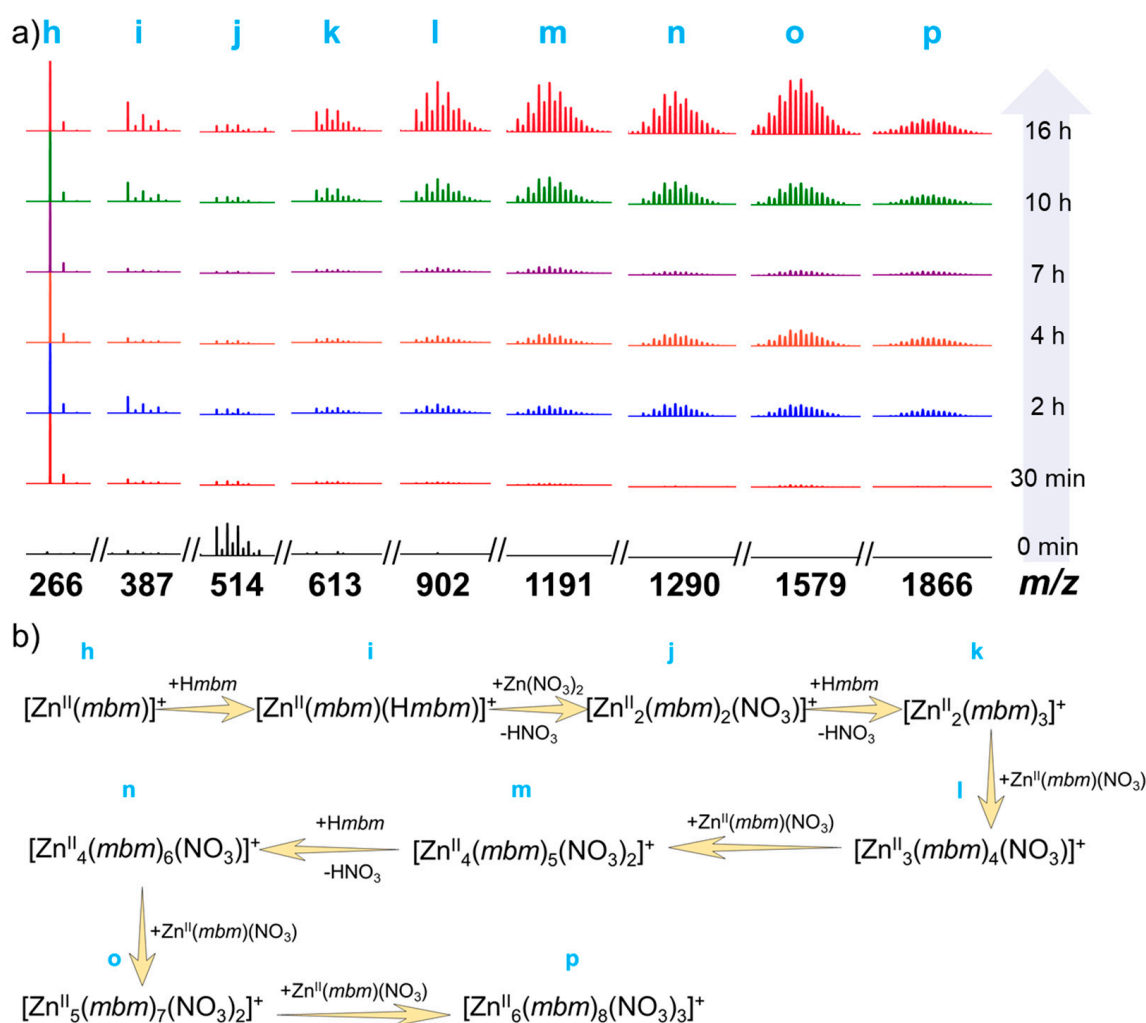


Figure 2. High resolution electrospray mass spectrometry (HRESI-MS) fragment (cationic mode) of cluster **Zn6** at different ion source energies (0–100 eV).

Furthermore, we analyzed the HRESI-MS test of **Zn6** in negative mode (Figures S5, S7 and Table S5). When the ion source voltage was 0 eV, the peak with the strongest peak was $m/z = 249.89$, which could be classified as $[\text{Zn}^{\text{II}}(\text{NO}_3)_3]^-$ (fit 249.89) by analysis. In addition, some other fragment peaks with low intensity were found such as $m/z = 348.98, 493.89, 507.91, 637.96, 737.05, 926.95, 1026.03, 1270.04, 1284.05, 1315.02, 1414.11, 1573.04, 1604.01,$ and 1703.09 , which were assigned as $[\text{Zn}^{\text{II}}(\text{mbm})(\text{NO}_3)_2]^-$ (fit 348.98), $[\text{Zn}^{\text{II}}_2(\text{mbm})(\text{NO}_3)_3(\text{OH})]^-$ (fit 493.89), $[\text{Zn}^{\text{II}}_2(\text{mbm})(\text{NO}_3)_3(\text{CH}_3\text{O})]^-$ (fit 507.91), $[\text{Zn}^{\text{II}}_2(\text{mbm})_2(\text{NO}_3)_3]^-$ (fit 637.96), $[\text{Zn}^{\text{II}}_2(\text{mbm})_3(\text{NO}_3)_2]^-$ (fit 737.05), $[\text{Zn}^{\text{II}}_3(\text{mbm})_3(\text{NO}_3)_4]^-$ (fit 926.95), $[\text{Zn}^{\text{II}}_3(\text{mbm})_4(\text{NO}_3)_3]^-$ (fit 1026.03), $[\text{Zn}^{\text{II}}_4(\text{mbm})_5(\text{NO}_3)_3(\text{OH})]^-$ (fit 1270.04), $[\text{Zn}^{\text{II}}_4(\text{mbm})_5(\text{NO}_3)_3(\text{CH}_3\text{O})]^-$ (fit 1284.05), $[\text{Zn}^{\text{II}}_4(\text{mbm})_5(\text{NO}_3)_4]^-$ (fit 1315.02), $[\text{Zn}^{\text{II}}_4(\text{mbm})_6(\text{NO}_3)_3]^-$ (fit 1414.10), $[\text{Zn}^{\text{II}}_5(\text{mbm})_6(\text{NO}_3)_4(\text{CH}_3\text{O})]^-$ (fit 1573.04), $[\text{Zn}^{\text{II}}_5(\text{mbm})_6(\text{NO}_3)_5]^-$ (fit 1604.01), and $[\text{Zn}^{\text{II}}_5(\text{mbm})_7(\text{NO}_3)_4]^-$ (fit 1703.09), respectively. The subject frame peak of **Zn6** was also not found in the anion mode, which also indicates that the cluster **Zn6** is prone to fracture under certain energy conditions.

Under the premise that the **Zn6** gradual fragmentation process is very clear, we tracked the assembly process (Figures S8–S11 and Table S6). When the ligands *Hmbm* and $\text{Zn}(\text{NO}_3)_2 \cdot 6\text{H}_2\text{O}$ were mixed, they reacted immediately, as shown by the black line (0 min) in Figure 3a. When not heated, the minimum building unit h $[\text{Zn}^{\text{II}}(\text{mbm})(\text{CH}_3\text{CN})]^+$ (fit 266.03) can be captured as well as the other small nuclear species peaks of i $[\text{HZn}^{\text{II}}(\text{mbm})_2]^+$ (fit 387.08), j $[\text{Zn}^{\text{II}}_2(\text{mbm})_2(\text{NO}_3)]^+$ (fit 513.99), and k $[\text{Zn}^{\text{II}}_2(\text{mbm})_3]^+$ (fit 613.07). When the reaction proceeded to 30 min, it could be seen that h became the strongest peak, indicating that the fragment was the most abundant, providing a raw material for further assembly to form a high-nuclear fragment; and the strength of j was reduced, indicating that in this process, j was further assembled into a fragment of a higher core number. When the reaction time was 2 h, we found new molecular ion peaks such as l $[\text{Zn}^{\text{II}}_3(\text{mbm})_4(\text{NO}_3)]^+$ (fit 902.10), m $[\text{Zn}^{\text{II}}_4(\text{mbm})_5(\text{NO}_3)_2]^+$ (fit 1191.04), n $[\text{Zn}^{\text{II}}_4(\text{mbm})_6(\text{NO}_3)]^+$ (fit 1290.13), o $[\text{Zn}^{\text{II}}_5(\text{mbm})_7(\text{NO}_3)_2]^+$ (fit 1579.11), and p $[\text{Zn}^{\text{II}}_6(\text{mbm})_8(\text{NO}_3)_3]^+$ (fit 1868.10). The high-nuclear fragments appeared gradually and the intensity increased, indicating that the small-nuclear species fragments gradually assembled into higher-nuclear species fragments as the reaction time progressed. As the reaction time continued to increase to 16 h, it could be seen that the abundance of the high-nuclear species fragments (k → p) gradually increased, indicating that as the reaction time increased, the raw materials gradually reacted and assembled into high-nuclear fragments, eventually forming clusters of **Zn6**. Based on HRESI-MS, the molecular ion peaks in the **Zn6** formation process solution were identified and the variation of molecular ion peaks was further analyzed. Herein, we propose the assembly process mechanism of the cluster **Zn6** (Figure 3b). Through its assembly mechanism, it can be found that there are many molecular ion peaks in the formation of **Zn6**, which were identical to the **Zn6** single crystal mass spectrum under different ion source conditions such as h, i, l, m, n, o, and p. Further analysis of the above peak intensity changes revealed that they all increased with time, indicating that the cluster **Zn6** gradually formed with time. Finally, the solution of the **Zn6** formation process at different time periods in the anion mode was followed (Figures S9, S11 and Table S6). We found that the species in the solution did not change significantly with time. Only the peak with $m/z = 249.89$ was observed. After analysis, it was assigned to $[\text{Zn}^{\text{II}}(\text{NO}_3)_3]^-$ (fit 249.89). No species peak changes associated with **Zn6** were observed. All in all, the gradual assembly mechanism of the cluster **Zn6** is $[\text{Zn}^{\text{II}}(\text{mbm})]^+ \rightarrow [\text{Zn}^{\text{II}}(\text{mbm})(\text{Hmbm})]^+ \rightarrow [\text{Zn}^{\text{II}}_2(\text{mbm})_2(\text{NO}_3)]^+ \rightarrow [\text{Zn}^{\text{II}}_2(\text{mbm})_3]^+ \rightarrow [\text{Zn}^{\text{II}}_3(\text{mbm})_4(\text{NO}_3)]^+ \rightarrow [\text{Zn}^{\text{II}}_4(\text{mbm})_5(\text{NO}_3)_2]^+ \rightarrow [\text{Zn}^{\text{II}}_4(\text{mbm})_6(\text{NO}_3)]^+ \rightarrow [\text{Zn}^{\text{II}}_5(\text{mbm})_7(\text{NO}_3)_2]^+ \rightarrow [\text{Zn}^{\text{II}}_6(\text{mbm})_8(\text{NO}_3)_3]^+ \rightarrow \text{Zn6}$ (Figure 3b).



2.3. Photoluminescence Properties

We dissolved the cluster **Zn6** in *N,N*-dimethylformamide (DMF) at room temperature and tested its UV–Visible absorption spectrum and photoluminescence spectrum. The UV–Vis absorption spectroscopy results showed that the cluster **Zn6** has strong absorption at 274 nm (Figure 4a). Further analysis of its photoluminescence showed that the excitation wavelength of the cluster **Zn6** was 285 nm, and the emission intensity peak at 300 nm and the emission shoulder peak at 600 nm were excited by the above wavelength (Figure 4b). Since the Zn(II) ion orbital electrons were in a fully charged state, which had no obvious influence on the luminescence, the above emission peak was mainly attributed to the π – π^* energy level transition of the ligand *Hmbm*. The above emission peaks indicated that **Zn6** mainly exhibits blue-green light emissions. When we excited the complex **Zn6** using the excitation wavelengths of 290 nm and 267 nm, respectively, there was no significant shift (Figure S12).

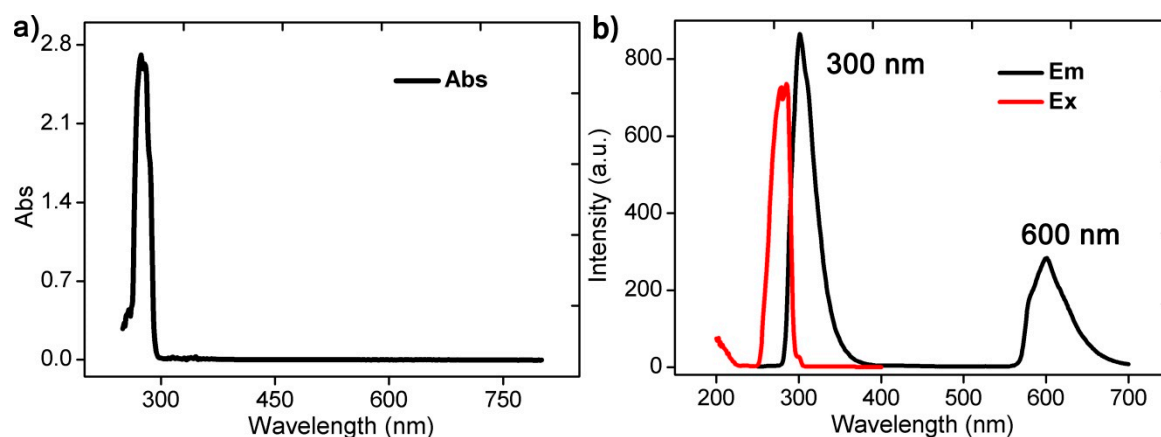


Figure 4. UV–Visible absorption spectroscopy (a) and photoluminescence spectrum (b) of the cluster **Zn6** dissolved in *N,N*-dimethylformamide (DMF) at room temperature.

3. Conclusions

In summary, we used a simple N,O chelating ligand (*Hmbm*) and Zn(II) ion reaction under solvothermal conditions to obtain a six-nuclear zinc cluster (**Zn6**) with five-coordinate Zn(II). Adjusting the high-resolution electrospray mass spectrometry (HRESI-MS) ion source energy observed a step by step decomposition of the cluster **Zn6**. Furthermore, HRESI-MS was used to track the changes of species in the reaction solution at different time periods during the formation of **Zn6**. Combined with the above decomposition process, we proposed a step by step assembly mechanism of **Zn6**. To the best of our knowledge, this is the first time that a decomposition and assembly binding strategy has been used to resolve the stepwise formation of Zn(II) clusters. Further photoluminescence tests indicate that the cluster **Zn6** mainly exhibits blue-green light emissions. This work provides a living example for analyzing the stepwise formation of high-nuclear clusters, further providing a basis for the design and synthesis of high-nuclear clusters.

4. Experimental Section

4.1. Materials and Measurements

All reagents were obtained from commercial sources and used without further purification. Elemental analysis (C, H, N) was measured on an Elementar Micro cube elemental analyzer. The thermal analysis was performed in N₂ at a heating rate of 5 °C/min using Labsys Evo TG-DTG/DSC. IR spectra with a KBr pellet were recorded on a PE Spectrum Two FT/IR spectrometer (400–4000 cm⁻¹). Powdered X-ray diffraction (PXRD) measurements were recorded on Rigaku D/max-III A diffractometer.

4.2. Single-Crystal X-Ray Crystallography

Diffraction data for all complexes were measured on a Bruker SMART CCD diffractometer (Mo K α radiation and $\lambda = 0.71073$ Å) in Φ and ω scan modes. All structures were solved by direct methods, followed by difference Fourier syntheses, and then refined by full-matrix least-squares techniques on F^2 using *SHELXL* [22]. All other non-hydrogen atoms were refined with anisotropic thermal parameters. Hydrogen atoms were placed in the calculated position and refined in the isotropic direction using a riding model. Table S1 summarizes the x-ray crystallographic data and refinement details for the complex. Full details can be found in the CIF files provided in the Supporting Information. The CCDC reference number is 1921550 for **Zn6**.

4.3. High Resolution Electrospray Mass Spectrometry (HRESI-MS) Test

High resolution electrospray mass spectrometry (HRESI-MS) were measured at the capillary temperature of 275 °C, and the solution was injected at the rate of 0.3 mL/h. The ESI-MS used for the

measurements was a ThermoExactive, and the data were collected in positive and negative ion modes. The spectrometer was previously calibrated with the standard tune mix to give a precision of *ca.* 2 ppm within the region of 200–2500 *m/z*. The capillary voltage was 50 V, the tube lens voltage was 150 V, and the skimmer voltage was 25 V. The in-source energy was set within the range of 0–100 eV with a gas flow rate at 10% of the maximum.

4.4. Synthesis of Cluster Zn6

We weighed 0.081 g (0.5 mmol) of *Hmbm* dissolved in 10 mL of CH₃CN, and then weighed 0.074 g (0.25 mmol) of Zn(NO₃)₂·6H₂O, which was added to the above solution. The mixture was stirred for 2 min and turbid. Finally, four drops of triethylamine (TEA) were added. The above solution was added to a 15 mL polytetrafluoroethylene reactor, reacted at 80 °C for 2 days (48 h), and slowly cooled to obtain a colorless transparent bulk crystal. The yield was 54.1% (based on Zn(NO₃)₂·6H₂O). The IR data for (KBr, cm⁻¹) were: 3415(m), 2945(w), 1636(w), 1485(s), 1458(m), 1376(s), 1075(m), 1003(w), 888(w), 754(m), 629(w), 537(w), and 476(w). The elemental analyses (%) for [Zn^{II}₆(*Hmbm*)₂(*mbm*)₈(NO₃)₄]·12H₂O·2CH₃CN are as follows: Theoretical value C, 44.27; H, 4.74; N, 14.28; Experimental value C, 44.34; H, 4.66; N, 14.22.

Supplementary Materials: The following are available online at <http://www.mdpi.com/2073-4352/9/8/416/s1>. Table S1: Crystallographic data of the complex **Zn6**, Table S2: Selected bond lengths (Å) and angles (°) of **Zn6**, Table S3: *SHAPE* analysis of the Zn^{II} ion in **Zn6**, Table S4: Intramolecular and intermolecular weak action of **Zn6**, Table S5: Analysis of molecular ion peaks of cluster **Zn6** in high resolution electrospray mass spectrometry (HRESI-MS) with different ion source voltages, Table S6: The HRESI-MS fragment of the cluster **Zn6** formation process was analyzed at different time periods, Figure S1: The intramolecular and intermolecular weak interaction of the cluster **Zn6**, Figure S2: Intermolecular stacking diagram of cluster **Zn6**, Figure S3: Cluster **Zn6** experiments and fitting PXRD patterns (a) and thermogravimetric analysis (b), Figure S4: HRESI-MS diagram of cluster **Zn6** under different ion source voltage conditions, Figure S5: HRESI-MS spectrum of cluster **Zn6** at 0 eV, Figure S6: The superposed simulated and observed spectra of several species for **Zn6** (Positive mode), Figure S7: The HRESI-MS spectrum of the reaction process of the cluster **Zn6** in different time periods (Positive mode), Figure S8: The HRESI-MS spectrum of the reaction process of the cluster **Zn6** in different time periods (Positive mode), Figure S9: The HRESI-MS spectrum of the reaction process of the cluster **Zn6** in different time periods (Negative mode), Figure S10: The superposed simulated and observed spectra of several species in the time-dependent ESI-MS of **Zn6** (Positive mode), Figure S11: The superposed simulated and observed spectra of several species in the time-dependent ESI-MS of **Zn6** (Negative mode), Figure S12: The emission peak (Em) obtained by exciting the DMF solution of the complex **Zn6** with excitation (Ex) wavelengths of 290 nm (a) and 267 nm (b), respectively.

Author Contributions: Conceptualization, Q.-J.D. and D.-C.C.; methodology, M.C.; software, C.-A.C.; validation, Q.-J.D. and D.-C.C.; formal analysis, M.C.; investigation, C.-A.C.; resources, Q.-J.D.; data curation, Q.-J.D.; writing-original draft preparation, M.C.; writing-review and editing, Q.-J.D.; visualization, M.C.; supervision, Q.-J.D.; project administration, Q.-J.D.; funding acquisition, Q.-J.D.

Funding: This work was supported by the Nature Science Foundation of China (No. 51872047), the key Project of Department of Education of Guangdong Province (2016GCZX008), and the Science and Technique Innovation Foundation of Foshan City (2017AB004041).

Conflicts of Interest: There are no conflicts of interest to declare.

References

1. Nevado, C.; de Haro, T. Synthetic Potential behind Gold-Catalyzed Redox Processes. In *New Strategies in Chemical Synthesis and Catalysis*; Wiley-VCH Verlag GmbH & Co. KGaA: Weinheim, Germany, 2012.
2. Sun, Q.F.; Sato, S.; Fujita, M. An M₁₈L₂₄ stellated cuboctahedron through post-stellation of an M₁₂L₂₄ core. *Nat. Chem.* **2012**, *4*, 330–333. [PubMed]
3. Miras, H.N.; Cooper, G.J.T.; Long, D.L.; Bögge, H.; Müller, A.; Streb, C.; Cronin, L. Unveiling the transient template in the self-assembly of a molecular oxide nanowheel. *Science* **2010**, *327*, 72–74. [CrossRef] [PubMed]
4. Guo, L.Y.; Su, H.F.; Kurmoo, M.; Tung, C.-H.; Sun, D.; Zheng, L.-S. Core-Shell [Mn7c(Mn, Cd) 12] Assembled from Core {Mn7} Disc. *J. Am. Chem. Soc.* **2017**, *139*, 14033–14036. [PubMed]
5. Deng, Y.K.; Su, H.F.; Xu, J.H.; Wang, W.-G.; Kurmoo, M.; Lin, S.-C.; Tan, Y.-Z.; Jia, J.; Sun, D.; Zheng, L.-S. Hierarchical assembly of a {MnII15MnIII4} brucite disc: step-by-step formation and ferrimagnetism. *J. Am. Chem. Soc.* **2016**, *138*, 1328–1334. [CrossRef] [PubMed]

6. Schröder, D. Applications of electrospray ionization mass spectrometry in mechanistic studies and catalysis research. *Acc. Chem. Res.* **2012**, *45*, 1521–1532. [[PubMed](#)]
7. Cook, T.R.; Stang, P.J. Recent developments in the preparation and chemistry of metallacycles and metallacages via coordination. *Chem. Rev.* **2015**, *115*, 7001. [[PubMed](#)]
8. Yu, G.C.; Zhang, M.M.; Saha, M.L.; Mao, Z.W.; Chen, J.; Yao, Y.; Zhou, Z.J.; Liu, Y.J.; Gao, C.Y.; Huang, F.H.; et al. Antitumor Activity of a Unique Polymer That Incorporates a Fluorescent Self-Assembled Metallacycle. *J. Am. Chem. Soc.* **2017**, *139*, 15940–15949. [[CrossRef](#)] [[PubMed](#)]
9. Zheng, H.; Du, M.-H.; Lin, S.-C.; Tang, Z.-C.; Kong, X.-J.; Long, L.-S.; Zheng, L.-S. Assembly of a Wheel-Like $\text{Eu}_{24}\text{Ti}_8$ Cluster under the Guidance of High-Resolution Electrospray Ionization Mass Spectrometry. *Angew. Chem. Int. Ed.* **2018**, *57*, 10976–10979. [[CrossRef](#)] [[PubMed](#)]
10. Zhu, Z.-H.; Ma, X.-F.; Wang, H.-L.; Zou, H.-H.; Mo, K.-Q.; Zhang, Y.-Q.; Yang, Q.-Z.; Li, B.; Liang, F.-P. A triangular Dy_3 single-molecule toric with high inversion energy barrier: magnetic properties and multiple-step assembly mechanism. *Inorg. Chem. Front.* **2018**, *5*, 3155–3162. [[CrossRef](#)]
11. Wang, H.-L.; Ma, X.-F.; Peng, J.-M.; Zhu, Z.-H.; Li, B.; Zou, H.-H.; Liang, F.-P. Tracking the Stepwise Formation of the Dysprosium Cluster (Dy_{10}) with Multiple Relaxation Behavior. *Inorg. Chem.* **2019**, *58*, 9169–9174.
12. Ma, X.-F.; Wang, H.-L.; Zhu, Z.-H.; Li, B.; Mo, K.-Q.; Zou, H.-H.; Liang, F.-P. Formation of nanocluster $\{\text{Dy}_{12}\}$ containing Dy-exclusive vertex-sharing $[\text{Dy}_4(\mu_3\text{-OH})_4]$ cubanes via simultaneous multitemplate guided and step-by-step assembly. *Dalton Trans.* **2019**, *48*, 11338–11344. [[CrossRef](#)]
13. Wang, H.L.; Peng, J.M.; Zhu, Z.H.; Mo, K.-Q.; Ma, X.-F.; Li, B.; Zou, H.-H.; Liang, F.-P. Step-by-Step and Competitive Assembly of Two Dy(III) Single-Molecule Magnets with Their Performance Tuned by Schiff Base Ligands. *Cryst. Growth Des.* **2019**. [[CrossRef](#)]
14. Yang, P.; Bassil, B.S.; Lin, Z.; Haider, A.; Alfaro-Espinoza, G.; Ullrich, M.S.; Silvestru, C.; Kortz, U. Organoantimony (III)-Containing Tungstoarsenates (III): From Controlled Assembly to Biological Activity. *Chem. - A Eur. J.* **2015**, *21*, 15600–15606. [[CrossRef](#)]
15. Zhou, J.; Du, X.; Xu, B. Regulating the Rate of Molecular Self-Assembly for Targeting Cancer Cells. *Angew. Chem. Int. Ed.* **2016**, *55*, 5770–5775. [[CrossRef](#)]
16. Wang, Q.M.; Lin, Y.M.; Liu, K.G. Role of anions associated with the formation and properties of silver clusters. *Acc. Chem. Res.* **2015**, *48*, 1570–1579. [[CrossRef](#)]
17. Brown, C.J.; Toste, F.D.; Bergman, R.G.; Raymond, K.N. Supramolecular catalysis in metal–ligand cluster hosts. *Chem. Rev.* **2015**, *115*, 3012–3035. [[CrossRef](#)]
18. Xu, F.; Miras, H.N.; Scullion, R.A.; Long, D.L.; Thiel, J.; Cronin, L. Correlating the magic numbers of inorganic nanomolecular assemblies with a $\{\text{Pd}_{84}\}$ molecular-ring Rosetta Stone. *Proc. Natl. Acad. Sci. USA* **2012**, *109*, 11609–11612. [[CrossRef](#)]
19. Kong, X.J.; Long, L.S.; Zheng, Z.; Huang, R.B.; Zheng, L.S. Keeping the ball rolling: Fullerene-like molecular clusters. *Acc. Chem. Res.* **2009**, *43*, 201–209. [[CrossRef](#)]
20. Saha, M.L.; Yan, X.; Stang, P.J. Photophysical properties of organoplatinum (II) compounds and derived self-assembled metallacycles and metallacages: Fluorescence and its applications. *Acc. Chem. Res.* **2016**, *49*, 2527–2539. [[CrossRef](#)]
21. Miras, H.N.; Wilson, E.F.; Cronin, L. Unravelling the complexities of inorganic and supramolecular self-assembly in solution with electrospray and cryospray mass spectrometry. *Chem. Commun.* **2009**, 1297–1311. [[CrossRef](#)]
22. Sheldrick, G.M. Crystal structure refinement with SHELXL. *Acta Crystallogr. Sect. C: Struct. Chem.* **2015**, *71*, 3–8. [[CrossRef](#)]

